Radiowave Propagation Characteristics of the Intra-Body Channel at 2.38 GHz

Radiowave Propagation Characteristics of the Intra-Body Channel at 2.38 GHz

Yomna El-Saboni, Gareth A. Conway, Simon L. Cotton, William G. Scanlon
Centre for Wireless Innovation (CWI), ECIT Institute
Queen's University Belfast, BT3 9DT, UK
yelsaboni01@qub.ac.uk, g.conway@qub.ac.uk, simon.cotton@qub.ac.uk, w.scanlon@qub.ac.uk

***Abstract*— Applications are emerging that feature multiple implanted devices as part of an intra-body network. Establishing high bandwidth communications between such devices is challenging and there is a need to understand the principles of the intra-body channel. This paper presents a numerical analysis of the wave propagation between identical antennas in the MedRadio operating band (2.36–2.40 GHz) within cylindrical three layered tissue equivalent phantoms. The results presented show the effect of dielectric boundaries and different tissue properties on dominant wave propagation paths and link gain which provides essential information for efficient system design.**

I. INTRODUCTION

Implantable Medical Device (IMD) applications can provide minimally invasive healthcare, offering benefits such as more comfortable post-surgery checkups through real time monitoring or home-based diagnosis [1]. Significant advances in microelectronics have allowed wireless IMDs to address many medical applications ranging from detection of temporary physiological abnormalities to regulation of long-term therapy, improving patients' quality of life and extending their independent living through smart prosthetics or artificial organs [2], [3]. While implantable systems suffer from a more challenging operating environment, they potentially offer access to better quality signals and more targeted actions or interventions.

However, as applications become more sophisticated, there is an emerging need for coordination between two or more IMD nodes, leading to the concept of the Intra-Body Network (IBN). The most basic example of where IBNs are needed is where the action of one implant is dependent on the signals received from a sensing element located elsewhere in the patient's body. Other examples include cases where communication relaying is required or some other form of co-operation or data sharing is needed. In some cases, the intra-body channel is short and less challenging since the implanted devices are relatively close to each other, e.g., in the case of a cochlear device or for a bionic eye where the sensory device is within centimeters away from the main implant. However, in other cases, the signal path is much longer and it may have to pass through several organs and different tissue types. For instance, for patients whom may have suffered from a stroke, spinal injury or chronic arthritis, establishing IBNs may allow a sensor placed in the spinal cord to connect with functional electrical stimulation implants in the limbs to restore movement.

II. THE RADIO FREQUENCY INTRA-BODY CHANNEL

For the implementation of IBNs, Radio Frequency (RF) links can be used to provide enhanced versatility and cable-free deployment [4]. In contrast to near field magnetic coupling or volume conduction alternatives [5], [6], the use of RF links for intra-body communication has the advantage of wider bandwidth and can safely penetrate tissue structures and organs to support the broadest range of possible IBN applications. Our focus here is on deeply implanted devices that need to communicate with each other within the same host body. Therefore, there is a need to study the essential principles of RF channels between IBN nodes and to understand how the characteristics of any specific application (e.g., the distance between implants, the tissues surrounding and between each implant and the effect of tissue boundaries) will affect IBN system design. Therefore, the intra-body channel is a major factor in setting the required radiation characteristics of the IMD antennas, operating frequency selection and achievable link performance. Furthermore, the intra-body channel is significantly sensitive to the location of the implants with respect to each other and surrounding tissue, which can vary with patient's age, weight and posture [7]. Some biological tissues have high electrical conductivity at RF frequencies that dramatically affects the signal attenuation and the path loss between devices [8]. In a numerical study [9], researchers tested implant antennas inside several different tissue equivalent phantoms with differing dielectric properties to gain more insight about the communication channel that can be established within the body. Subsequently, the same authors considered the propagation between implants inside a phantom and compared it with a single implant case and its communication with an external device [10]. However, these studies were carried out using different single layered phantoms, and multilayered phantoms were not considered.

In an early numerical study [11], the intra-body channel was shown to suffer from significant attenuation losses due to the lossy tissue properties of the human body. More recent work [12] shows that the RF link between implantable antennas experiences dramatic reflection, refraction and transmission losses depending on the dielectric properties of the tissues, the boundary shape and the angle of wave. Furthermore, the dielectric properties of the local tissue environment significantly affects the performance of the implant antenna and its resonating frequency [13]. This places another restriction on the design of narrow band antennas, as they may need to be modified and tuned each

time their position changes with respect to its medium. To solve this issue, multi-resonance antenna solutions have been proposed [14].

In this paper, we consider a generic intra-body channel by numerically investigating the radiowave propagation between two identical implant antennas within a multi-layered cylindrical tissue equivalent phantom. We study the effect of implant antenna separation and the effect of changing the surrounding tissue boundaries on the overall channel gain and dominant propagation paths.

III. Numerical Modelling

The numerical study was performed in CST Microwave Studio® using layered cylindrical tissue phantoms and two identical bowtie dipole antennas. A geometrical phantom design was chosen to help illustrate wave propagation through several different tissue boundaries. The cylindrical numerical phantoms had a muscle core, concentric fat mid layer and skin outer layer. The outer diameter and height of the cylindrical phantom were set at 300 mm and 340 mm, respectively. However, the position of the muscle-fat boundary was varied to understand its effect on the channel path loss. A bone core was added to one of the phantoms as an additional propagation scenario. The tissue properties used are shown in Table I.

A. Frequency Band

The MedRadio Band (2.36-2.4 GHz) [15] was chosen for this study as there is increasing interest in wideband IBN solutions to accommodate the future development of intelligent sensing systems and real time responsive medical systems. Furthermore, the higher losses at this frequency make the results more distinctive and therefore help draw out the principles of electromagnetic wave propagation affecting the intra-body channel.

B. Antenna Design

An insulated bowtie dipole antenna was selected for this study as its broader resonant bandwidth makes it possible to use the same antenna across the different tissue types without retuning. The antenna dimensions were optimized using three different homogenous phantoms; muscle, fat and skin. A single antenna was placed at the center of each phantom and the physical dimensions adjusted to ensure that it remained matched ($|S_{11}| < -10$ dB) across the MedRadio band. The total height (h) and width (w) of the antenna were 26.4 mm and 33.0 mm, respectively, with a delta gap source ∂ = 0.2 mm, as illustrated in Fig. 1. The antenna was modelled as a perfect electric conductor with thickness (k) of 0.2 mm and an insulation all-round thickness (t) of 1.6 mm. The insulation material was chosen to be vacuum to represent a lossless coating.

TABLE I TISSUE PROPERTIES AT 2.38 GHz

Tissue Type	Relative Permittivity (ε_r)	Conductivity (σ) (S/m)
Muscle	52.8	1.69
Fat	5.29	0.10
Skin	38.1	1.43
Bone	11.4	0.38

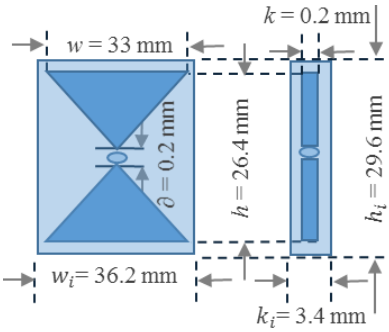

Fig. 1 Schematic (front view and side view) of insulated bowtie antenna.

C. Simulation Set-up

The study utilized three multilayered phantoms, each with muscle diameter D_M, fat diameter D_F and total diameter D_T (Fig. 2). Phantom 1 had a muscle core of radius 135 mm with 10 mm additional radius of fat tissue (to 145 mm) and then 5 mm additional radius of skin (150 mm). Phantom 2 had a muscle core of radius 125 mm with 20 mm additional radius of fat tissue (to 145 mm) and the same 5 mm of skin. Phantom 3 had a muscle core of radius 100 mm with 45 mm additional radius of fat and 5 mm of skin. Furthermore, a variant of Phantom 2 was simulated including a bone core that had a radius of 12.5 mm. The simulations were performed with the antennas positioned symmetrically with respect to each phantom at various separations along the z-axis beginning within the muscle tissue at 5 mm radius and ending 15 mm outside the phantom (radius of 165 mm, separation of 330 mm). The antennas were oriented vertically within the cylinder (parallel to the x-axis) with the top and bottom edges of the bowtie parallel to the y-axis. In the analysis Region 1 refers to the case where the antennas are well inside the muscle core (radius 5-70 mm); Region 2 is when the antennas are either close to or within the fat layer depending on the phantom (radius 71-130 mm); Region 3 is the area surrounding the skin layer (radius 131-150 mm) and Region 4 is when the antennas are outside the phantom and in the air (radius 151-165 mm).

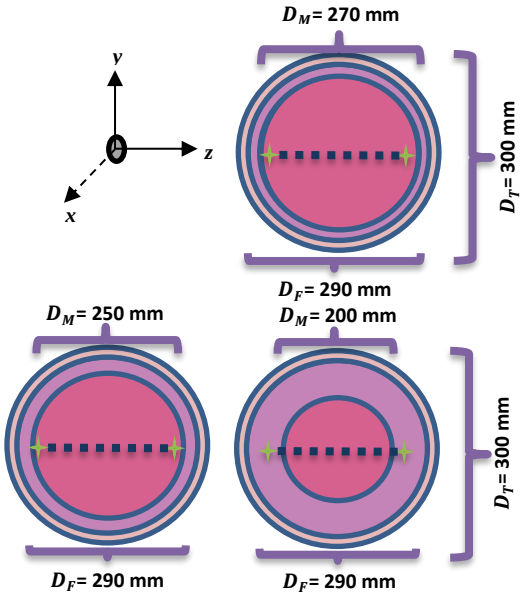

Fig. 2 Schematic of the antenna arrangement inside Phantom 1 (top), Phantom 2 (bottom left) and Phantom 3 (bottom right).

IV. Results

A. Electric Field Distribution

The antennas were simulated within the three different phantoms and the electric field (E_x) distribution at 2.38 GHz in the perpendicular (y-z) plane of the cylindrical phantom is shown in Fig. 3. The plots demonstrate the wave propagation across the 4 different regions described in Section III. The main transfer mechanism is through far field wave propagation since all cases presented are separated by more than 2λ in muscle tissue at 2.38 GHz (2 x 17 mm). Each row represents a selected position within each region. The only difference between each column in Fig. 3 is the thicknesses of the fat layer and hence the position of the muscle / fat boundary and the presence of a bone core in the third column. In Region 1 (65 mm), there is direct propagation from the excited antenna (on the right) to the second antenna (on the left) irrespective of the position of the muscle / fat boundary. The muscle tissue losses are significant but the antennas are close enough together for the direct path to be dominant. However, for Phantom 3, the broader (and therefore closer) fat layer allows secondary propagation around the circumference of the cylinder, which results in an interference pattern within the muscle region. For Region 2 (105 mm), the antennas in the Phantom 1 and 2 cases are still in muscle but in Phantom 3 both antennas are in just within the fat region. This results in a significant guided wave through the fat layer for the Phantom 3 case and higher overall field levels due to the lower near-field losses experienced by the excited antenna. Furthermore, the fields outside Phantom 3 are significantly larger than the other two cases. In the Region 3 case (140 mm), the antennas are within the fat layer in all Phantoms and the guided wave effect is apparent for each. For the Region 4 case (156 mm), the antennas are in air in all cases, but the thicker fat layers in Phantoms 2 and 3 lead to reduced creeping wave losses compared to the case where the muscle layer is close to the surface in Phantom 1.

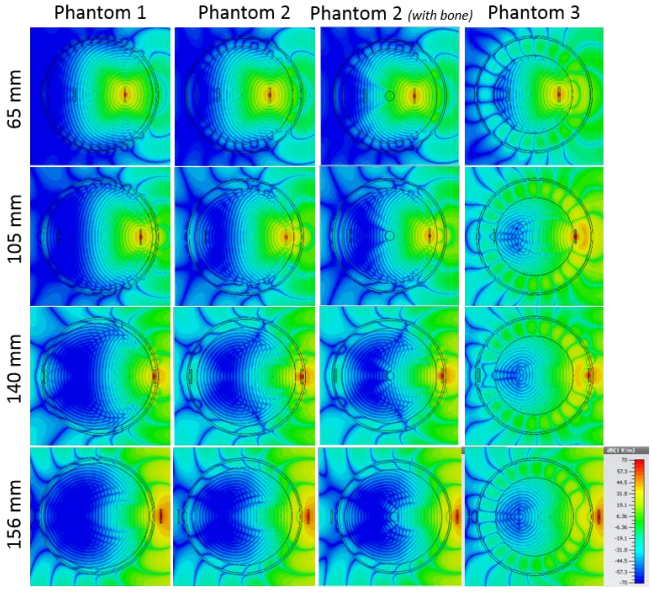

Fig. 3 Electric field (E_x) distribution at 2.38 GHz for the different multi-layer phantoms.

TABLE II FORWARD PATH GAIN IN REGIONS 1-4 AT 2.38 GHz

Position	$\|S_{21}\|$ **(dB)**	**Phantom 1**	**Phantom 2**	***Phantom 2 with bone***	**Phantom 3**
65 mm		–96.4	–96.6	*–97.5*	–96.8
105 mm		–118.5	–103.4	*–104.4*	–76.9
140 mm		–83.8	–76.5	*–76.5*	–76.8
165 mm		–112.5	–94.9	*–94.9*	–94.8

B. Forward Path Gain

Table II gives the forward path gain ($|S_{21}|$) for each of the cases shown in Fig 3. The results highlight the difference between the phantom types and the effect of the antenna position. Although the forward gain is the same in all phantoms when the antenna is in Region 1, there is up to 42 dB improvement for Phantom 3 in Region 2 caused by a combination of the lower antenna near field losses and wave guiding in the fat layer. For Regions 3 and 4, Phantoms 2 and 3 have almost equal forward gain values confirming that the main propagation path is now around the circumference of the phantom through both the fat and air layers. Additionally, there was a small reduction in path gain when the bone core was added but no change for Regions 3 and 4 which suggests that the main propagating path is through the outer layers rather than through the direct path between the antennas. Moreover, it is noted that, irrespective of the phantom considered, the results for 140-mm (280 mm antenna separation) are significantly (> 20 dB) better than the 65-mm case (130 mm separation) which demonstrates the complexity of intra-body channels.

Fig. 4 shows more detailed forward path gain results for each phantom. The position of the skin and air boundaries is shown and is independent of phantom. The position of the muscle/fat boundary is shown for each phantom. The graph highlights the difference in wave propagation as the position of the antennas changes and how this varies with the change in tissue boundaries. In all cases, there is a clear turning point in the expected decline in forward path gain as the antennas are further separated. This occurs at a point where the non-direct path starts to dominate. For Phantom 3 this happens at 78 mm radius and at 92 mm for the other phantoms. Fig. 4 also illustrates the much lower gain in the skin region which is a combination of high near field antenna losses and the proximity of two significant impedance boundaries (fat/skin and skin/air). It is also interesting that the Region 4 (antennas in air) performance is equal for Phantoms 2 and 3 but it is significantly poorer for Phantom 1. This is due to the additional losses incurred by the creeping wave with the proximity of the muscle layer to the surface of the phantom.

V. Discussion

The results presented provide significant insight into the nature of the propagation channel between implanted antennas. The electric field distribution plots obtained from simulations of identical bowtie antennas inside multi-layered phantoms (Fig. 2) demonstrate the challenges faced with establishing efficient communication links between implanted devices, particularly deep within the body tissues. The results demonstrate how antenna radiation propagates along different paths depending on the surrounding tissues and the implant position with respect to the outside of the phantom, even in this simplified geometric representation.

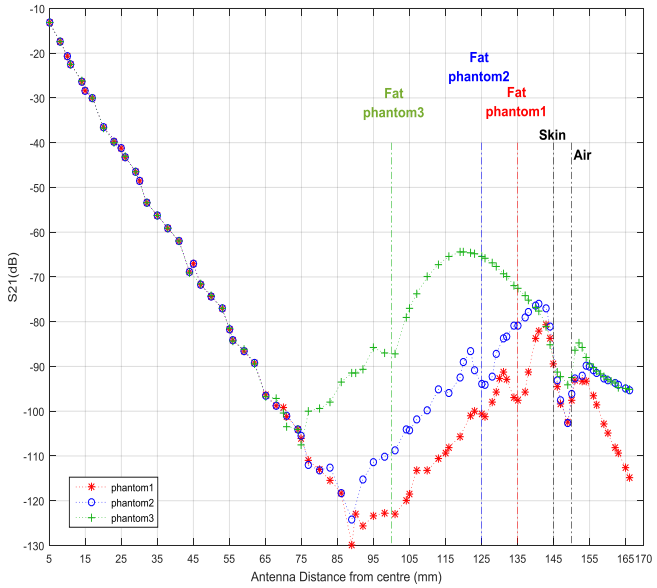

Fig. 4 Forward gain ($|S_{21}|$) for link between the insulated bowtie dipoles at different positions. The symbol color indicates the phantom.

In the cases where the antennas are relatively close together (e.g., in Region 1), the lossy muscle tissue leads to poor direct path gain but the losses also ensure that the energy available to flow along the "around the periphery" path is insignificant. This means that the forward path gain in Region 1 remains similar for all three phantoms despite the change in the muscle/fat boundary position.

Interestingly, the results in Fig. 4 show that, for implants closer to the surface, the forward path gain peaks in the fat layer in all cases irrespective of the layer's width since the strong material discontinuities (muscle/fat; fat/skin; skin/air) tend to guide the propagating wave around the body. However, when the antennas are in air, the skin/air interface causes a significant scattering of energy in the off-body direction and connectivity is only maintained through a surface creeping wave which is highly attenuated by the skin and muscle layers, particularly in the case of Phantom 1 where the muscle layer is close to the phantom surface.

Additionally, the Phantom 3 results in Fig. 4 demonstrate the effect of material boundaries on the forward path gain performance. In Region 2 the path gain steadily increases to a peak then falls again. The peak gain of –64 dB occurs close to the middle of the fat layer (~120 mm radius). Furthermore, the forward gain in Regions 3 and 4 remains almost the same in Phantom 2 and 3, despite the 25-mm additional radius of fat tissue. This strongly indicates that in IBNs a single path becomes dominant and performance is then largely independent of material boundaries outside of this path. This agrees with the analysis discussed in [12].

VI. Conclusion

This numerical study demonstrates the challenges facing intra-body network designers due to relatively poor path gains associated with the intra-body channel. However, the work also highlights the opportunity for smarter system design, depending on the needs and restrictions of the application being considered, since IBNs may be supported by non-direct propagating paths. The results also illustrate the effect of varying tissue boundaries both within and outside the direct intra-body path. For the cases considered, there is always a point where wave propagation is predominantly around the periphery of the phantom rather than through the center of the phantom. Future work will consider these effects at other frequencies and will consider how best to design the radiation characteristics of antennas to maximize link gain. For example, directional antenna designs may be used to direct radiation towards the surface layers of the body to utilize the guided wave effect and avoid high "through-body" losses. Finally, it is intended to validate this work through empirical testing using a suitable multi-layered tissue phantom test bed.

References

[1] R. S. Alrawashdeh, Yi Huang, M. Kod, and A. Abu Bakar Sajak, "A Broadband Flexible Implantable Loop Antenna With Complementary Split Ring Resonators," *IEEE Antennas Wireless Propagation Lett.*, vol. 14, pp. 1506–1509, 2015.

[2] C. Garcia-Pardo, A. Fornes-Leal, N. Cardona, R. Chavez-Santiago, J. Bergsland, I. Balasingham, S. Brovoll, O. Aardal, S.-E. Hamran, and R. Palomar, "Experimental ultra wideband path loss models for implant communications," in *IEEE 27th Ann. Intl. Symp. on Personal, Indoor, and Mobile Radio Communications (PIMRC)*, 2016, pp. 1–6.

[3] A. Valanarasi and R. Dhanasekaran, "A review on design considerations of implantable antennas," in *2016 International Conference on Advanced Communication Control and Computing Technologies (ICACCCT)*, 2016, pp. 207–211.

[4] A. Venkatasubramanian and B. Gifford, "Modeling and design of antennas for implantable telemetry applications," in *2016 38th Annual International Conference of the IEEE Engineering in Medicine and Biology Society (EMBC)*, 2016, pp. 6469–6472.

[5] T. G. Zimmerman, "Personal Area Networks: Near-field intrabody communication," *IBM Systems J.*, vol. 35, no. 3.4, pp. 609–617, 1996.

[6] H. Baldus, S. Corroy, A. Fazzi, K. Klabunde, and T. Schenk, "Human-centric connectivity enabled by body-coupled communications," *IEEE Commun. Mag.*, vol. 47, no. 6, pp. 172–178, Jun. 2009.

[7] M. Patel and J. Wang, "Applications, challenges, and prospective in emerging body area networking technologies," *IEEE Wireless Commun.*, vol. 17, no. 1, pp. 80–88, Feb. 2010.

[8] E. Chow, M. Morris, and P. Irazoqui, "Implantable RF Medical Devices: The Benefits of High-Speed Communication and Much Greater Communication Distances in Biomedical Applications," *IEEE Microwave Magazine*, vol. 14, no. 4, pp. 64–73, Jun. 2013.

[9] A. Khaleghi, I. Balasingham, and R. Chavez-Santiago, "An ultra-wideband wire spiral antenna for in-body communications using different material matching layers," in *36th Ann. Intl. Conf. of the IEEE Engineering in Medicine & Biology Soc.*, 2014, pp. 6985–6988.

[10] R. Chavez-Santiago, C. Garcia-Pardo, A. Fornes-Leal, A. Valles-Lluch, G. Vermeeren, W. Joseph, I. Balasingham, and N. Cardona, "Experimental Path Loss Models for In-Body Communications within 2.36-2.5 GHz," *IEEE J. Biomed. Health Informatics*, vol. 19, no. 3, pp. 1–1, 2015.

[11] W. G. Scanlon, "Analysis of tissue-coupled antennas for UHF intra-body communications," in *Twelfth Intl. Conference on Antennas and Propagation (ICAP 2003)*, 2003, vol. 2003, pp. 747–750.

[12] Y. El-Saboni, G. A. Conway, and W. G. Scanlon, "Effect of Tissue Boundaries on The Intra-Body Communication Channel at 2.38 GHz," in *Intl. Workshop on Antenna Technology (iWAT)*, 2017.

[13] A. Khaleghi and I. Balasingham, "On selecting the frequency for wireless implant communications," in *Loughborough Antennas & Propagation Conference (LAPC)*, 2015, pp. 1–4.

[14] M. K. Magill, G. A. Conway, and W. G. Scanlon, "Robust implantable antenna for in-body communications," *Loughborough Antennas Propag. Conf. LAPC 2015*, pp. 1–12, 2015.

[15] "Medical Device Radiocommunications Service (MedRadio) | Federal Communications Commission," *Wireless Telecommunications*, 2016. Available: https://www.fcc.gov/general/medical-device-radiocommunications-service-medradio. [Accessed: 07-Aug-2016].